Hydrol. Earth Syst. Sci. Discuss., 12, 8419–8457, 2015
www.hydrol-earth-syst-sci-discuss.net/12/8419/2015/
doi:10.5194/hessd-12-8419-2015

Hydrology and Earth System Sciences Discussions
Open Access

The Normalized Difference Infrared Index (NDII) as a proxy for soil moisture storage in hydrological modelling

N. Sriwongsitanon[1], H. Gao[2], H. H. G. Savenije[2], E. Maekan[1], S. Saengsawang[1], and S. Thianpopirug[1]

[1]Department of Water Resources Engineering, Faculty of Engineering, Kasetsart University, Bangkok, Thailand
[2]Water Resources Section, Delft University of Technology, Delft, the Netherlands

Received: 16 July 2015 – Accepted: 22 July 2015 – Published: 27 August 2015

Correspondence to: N. Sriwongsitanon (fengnns@ku.ac.th)

Published by Copernicus Publications on behalf of the European Geosciences Union.

Abstract

With remote sensing we can readily observe the Earth's surface, but looking under the surface into the root zone of vegetation is still a major challenge. Yet knowledge on the dynamics of soil moisture in the root zone is essential for agriculture, land–atmosphere interaction and hydrological modelling, alike. In this paper we develop a novel approach to monitor the soil moisture storage deficit in the root zone of vegetation, by using the remotely sensed Normalised Difference Infrared Index (NDII) in the Upper Ping River Basin (UPRB) in northern Thailand. Satellite data from the Moderate Resolution Imaging Spectro-radiometer (MODIS) was used to evaluate the NDII over an 8 day period, covering the study area from 2001 to 2013. The results show that NDII values decrease sharply at the end of the wet season in October and reach lowest values near the end of the dry season in March. The values then increase abruptly after rains have started, but vary in an insignificant manner from the middle to the late rainy season. The NDII proves to be a very strong proxy for moisture storage deficit in the root zone, which is a crucial component of hydrological models. In addition, the NDII appears to be a reliable indicator for the temporal and spatial distribution of drought conditions in the UPRB. The 8 day average NDII values were found to correlate very well with the 8 day average soil moisture content (S_U) simulated by FLEX^L (rainfall–runoff model) at 8 runoff stations during the dry season – giving an average R^2 value 0.87 on an exponential relationship, while for the wet season it reduced to be around 0.61.

Apparently, the NDII is an effective index for the moisture storage in the root zone during the time of moisture deficit, and a powerful indicator to assess droughts. In the dry season, when plants are exposed to water stress, the leaf-water deficit increases steadily. Once leaf-water is close to saturation – mostly at the end of the wet season – leaf characteristics and NDII values do not vary significantly, causing lower correlation between NDII and S_u in the wet season. However, the correlations between NDII and S_u still remain high for both seasons and therefore the product can be used to define drought situations throughout the year and be of use to water management.

HESSD
12, 8419–8457, 2015

1 Introduction

Estimating the moisture content of the soil from remote sensing is one of the main challenges in the field of hydrology (e.g. De Jeu et al., 2008; Entekhabi et al., 2010). Soil moisture is generally seen as the key hydrological state variable determining the partitioning of fluxes (into direct runoff, recharge and evaporation) (Liang et al., 1994), the interaction with the atmosphere (Legates et al., 2011), and the carbon cycle (Porporato et al., 2004). The part of the soil that is key in all these processes is the root zone of vegetation, which is the dynamic part of the unsaturated zone. Several remote sensing products have been developed especially for monitoring soil moisture (e.g. SMOS, ERS and AMSR-E), but until now correlations between remote sensing products and observed soil moisture at different depths have been modest at best (Parajka et al., 2006; Ford et al., 2014). There are a few possible explanations. One is that it is not (yet) possible to look into the soil deep enough to observe soil moisture in the root zone of vegetation (Shi et al., 1997), second is that soil moisture observations at certain depths are maybe not the right indicators for the storage in the root zone (Mahmood and Hubbard, 2007).

In this paper we try to relate a remote sensing product (the NDII) to the root zone storage of a conceptual hydrological model, as a key state variable in the short and long term dynamics of the rainfall–runoff signal. In order to do so, we calibrated a conceptual rainfall–runoff model to observed time series in the Upper Ping basins in Thailand and subsequently compared the temporal variability of the root zone storage to the NDII. A popular remote sensing product connected to vegetation performance is the Normalized Difference Vegetation Index (NDVI), introduced by Rouse et al. (1974). NDVI can be derived from spectral reflectance data (ρ) of discrete red (R) and near-infrared (NIR) channels such as $(\rho_{\text{NIR}} - \rho_{\text{RED}})/(\rho_{\text{NIR}} + \rho_{\text{RED}})$ (Rhee et al., 2010). The contrast between intense chlorophyll pigment absorption in the red channel and high reflectance of leaf mesophyll in the near infrared channel is the main characteristic used for operating NDVI. It can be used to indicate vegetation stress, particularly due

HESSD
12, 8419–8457, 2015

to water shortage, which is a main factor affecting vegetation and controls leaf pigment content and integrity (Maselli, 2004). Being an indicator for photosynthetic activity in the plant, the NDVI appears to be a good proxy for the actual transpiration of an ecosystem (e.g. Wang et al., 2007; Gao et al., 2014b).

The Normalized Difference Infrared Index (NDII) was later developed by Hunt and Rock (1989) using ratios of different values of near infrared reflectance (NIR) and short wave infrared reflectance (SWIR), and, similar to the NDVI, defined by: $(\rho_{\text{NIR}} - \rho_{\text{SWIR}})/(\rho_{\text{NIR}} + \rho_{\text{SWIR}})$. NDII can be effectively used to detect plant water stress according to the property of shortwave infrared reflectance, which is negatively related to leaf water content due to the large absorption by the leaf (e.g. Steele-Dunne et al., 2012; Friesen et al., 2012; Van Emmerik et al., 2015). Many studies have found relationships between the equivalent water thickness (EWT) and reflectance at the near-infrared (NIR) and shortwave infrared (SWIR) portion of the spectrum used for deriving NDII (Hunt and Rock, 1989; Gao, 1996; Ceccato et al., 2002; Fensholt and Sandholt, 2003). Yilmaz et al. (2008) found a significant relationship ($R^2 = 0.85$) between equivalent water thickness (EWT) and NDII. They also discovered a significant indirect relationship between NDII and vegetation water content (VWC), which is the most successful parameter for retrieval of soil moisture content from microwave data, based on the allometric relationships between canopy EWT and VWC, and the linear relationship between canopy EWT and NDII. Fensholt and Sandholt (2003) derived a shortwave infrared water stress index (SIWSI or NDII) on a daily basis and found a strong correlation with in situ top layer soil moisture measurements from the semiarid Senegal in 2001 and 2002. NDII was therefore selected in this study of the Upper Ping River Basin (UPRB) in northern Thailand because of its potential in detecting equivalent water thickness within the leaves affected by soil moisture storage in the root zone. The relationship between average NDII and root zone moisture storage was evaluated at the 14 sub-basins of the UPRB to be used as an indicator to prove the effectiveness of NDII. However, because the NDII is an indicator for water stress, the index is only expected to show a strong link to moisture storage in the root zone when there

HESSD
12, 8419–8457, 2015

is a soil moisture deficit. Without water stress occurring within the leafs, particularly during the end of the wet season, NDII would possibly not reflect changes in root zone soil moisture content (Korres et al., 2015).

Instead of comparing the NDII to observed soil moisture by in field instrumentation, here another approach has been followed. To acquire the information on root zone soil moisture, the lumped (basin average) FLEX^L conceptual hydrological rainfall–runoff model (Fenicia et al., 2011; Gao et al., 2014a, b) was used and calibrated on 8 runoff stations in sub-basins of the UPRB. The simulated root zone storage variation was then compared to the sub-basin average NDII values over the 8 sub-basins.

2 Methods

2.1 Estimating vegetation water content using near infrared and short wave infrared

Estimates of vegetation water content (the amount of water in stems and leaves) are of interest to assess the vegetation water status in agriculture and forestry and have been used for drought assessment (Cheng et al., 2006; Gao, 1996; Gao and Goetz, 1995; Ustin et al., 2004; Peñuelas et al., 1993). Evidence of physically based radiative transfer models and laboratory studies have proved that changes in water content in plant tissues have a large effect on the leaf reflectance in several regions of the 700–2500 nm spectrum (Fensholt and Sandholt, 2003). Tucker (1980) suggested that the spectral interval between 1550 and 1750 nm (SWIR) is the most suitable region for remotely sensed leaf water content. It is well known that these wavelengths are negatively related to leaf water content due to a large absorption by leaf water (Tucker, 1980; Ceccato et al., 2002). However, variations in leaf internal structure and leaf dry matter content also influence the SWIR reflectance. Therefore, only SWIR reflectance values are not suitable for retrieving vegetation water content. To improve the accuracy in retrieving the vegetation water content, a combination of SWIR and NIR (700 to 900 nm)

HESSD
12, 8419–8457, 2015

N. Sriwongsitanon et al.

reflectance information was utilized because NIR is only affected by leaf internal structure and leaf dry matter content but not by water content. A combination of SWIR and NIR reflectance information can remove the effect of leaf internal structure and leaf dry matter content and can improve the accuracy in retrieving the vegetation water content (Ceccato et al., 2001; Yilmaz et al., 2008; Fensholt and Sandholt, 2003).

On the basis of this idea, Fensholt and Sandholt (2003) derived a shortwave infrared water stress index (SIWSI or NDII) on a daily basis and found a strong correlation with in situ top layer soil moisture measurements in semiarid Senegal in 2001 and 2002,

$$\mathrm{NDII} = \frac{\rho_{0.85} - \rho_{1.65}}{\rho_{0.85} + \rho_{1.65}} \tag{1}$$

where $\rho_{0.85}$ and $\rho_{1.65}$ are the reflectances at 0.85 and 1.65 µm wavelengths, respectively. NDII is a normalized index and the values theoretically vary between −1 and 1. A low NDII value and especially below zero means that reflectance from $\rho_{0.85}$ is higher than the reflectance from $\rho_{1.65}$ and this indicates canopy water stress.

2.2 FLEX$^{\mathrm{L}}$ model

FLEX$^{\mathrm{L}}$ (Fig. 1) is a lumped conceptual hydrological model which has an HBV-like model structure developed in a flexible modelling framework (Fenicia et al., 2011; Gao et al., 2014a, b). The model structure comprises four conceptual reservoirs: the interception reservoir S_{i} (mm), the unsaturated reservoir representing the moisture storage in the root zone S_{u} (mm), the fast response reservoir S_{f} (mm), and the slow response reservoir S_{s} (mm). It also includes two lag functions representing the lag time from storm to peak flow (T_{lagF}), and the lag time of recharge from the root zone to the groundwater (T_{lagS}). Besides a water balance equation, each reservoir has process equations that connect the fluxes entering or leaving the storage compartment to the storage in the reservoirs (so-called constitutive functions). Table 1 shows 15 mathematical expressions used for modelling the FLEX$^{\mathrm{L}}$. A total of 11 model parameters with their distribution values are shown in Table 2 and they have to be identified by model calibration.

HESSD
12, 8419–8457, 2015

Forcing data include the elevation-corrected daily average rainfall, daily average, minimum and maximum air temperature, and potential evaporation.

2.2.1 Interception reservoir

The interception evaporation E_i (mm d^{-1}) is calculated by potential evaporation E_0 (mm d^{-1}) and the storage of the interception reservoir S_i (mm d^{-1}) (Eq. 3). There is no effective rainfall P_e (mm d^{-1}) as long as the S_i is less than its storage capacity $S_{i,\,max}$ (mm) (Eq. 4) (de Groen and Savenije, 2006).

2.2.2 Unsaturated root zone reservoir

The unsaturated root zone reservoir partitions effective rainfall into infiltration, and runoff R (mm d^{-1}), and determines the transpiration by vegetation. Therefore, it is the core of the FLEX^{L} model. In this study, we applied the widely used beta function (Eq. 6) of the Xinanjiang model (Zhao, 1992) to compute the runoff coefficient C_r (–) for each time step as a function of the relative soil moisture content ($S_u/S_{u,\,max}$). In Eq. (6), $S_{u,\,max}$ (mm) is the root zone storage capacity, and β (–) is the shape parameter describing the spatial distribution of the root zone storage capacity over the catchment. In Eq. (7), the relative soil moisture and potential evaporation are used to determine the transpiration E_t (mm d^{-1}); C_e (–) indicates the fraction of $S_{u,\,max}$ above which the transpiration is no longer limited by soil moisture stress ($E_t = E_0 - E_i$).

2.2.3 Response routine

In Eq. (8), R_f (mm d^{-1}) indicates the flow into the fast response routine; D (–) is a splitter to separate recharge from preferential flow. In Eq. (9), R_s (mm d^{-1}) indicates the flow into the groundwater reservoir. Equations (10) and (11) are used to describe the lag time between storm and peak flow. R_f $(t - i + 1)$ is the generated fast runoff from the unsaturated zone at time $t - i + 1$; T_{lag} is a parameter which represents the time lag

HESSD
12, 8419–8457, 2015

between storm and fast runoff generation; $c(i)$ is the weight of the flow in $i-1$ days before; and $R_{\mathrm{fl}}(t)$ is the discharge into the fast response reservoir after convolution.

The linear response reservoirs, representing linear relationships between storages and releases, are applied to conceptualize the discharge from the surface runoff reservoir, fast response reservoir and slow response reservoir. In Eq. (12), Q_{ff} (mm d^{-1}) is the surface runoff, with timescale K_{ff} (d), activated when the storage of fast response reservoir exceeds the threshold $S_{\mathrm{f,\,max}}$ (mm). In Eqs. (14) and (16), Q_{f} (mm d^{-1}) and Q_{s} (mm d^{-1}) represent the fast and slow runoff; K_{f} (d) and K_{s} (d) are the time scales of the fast and slow runoff, respectively. Q_m (mm d^{-1}) is the total amount of runoff simulated from the three individual components, including Q_{ff}, Q_{f}, and Q_{s}.

2.3 Model calibration method

2.3.1 Objective functions

A multi-objective calibration strategy has been adopted in this study to allow for the model to effectively reproduce different aspects of the hydrological response, i.e. high flow, low flow and the flow duration curve. The model was therefore calibrated to three Kling-Gupta efficiencies (Gupta et al., 2009): (1) the overall K-G efficiency of flows (I_{KGE}) that measures primarily the performance during high flows, (2) the K-G efficiency of the logarithm of flows that emphasizes low flows (I_{KGL}), and (3) the K-G efficiency of the flow duration curve (I_{KGF}) to evaluate the modelled flow frequency dynamics.

2.3.2 Model calibration

The MOSCEM-UA (Multi-Objective Shuffled Complex Evolution Metropolis-University of Arizona) algorithm (Vrugt et al., 2003) was used as the calibration algorithm to find the Pareto-optimal solutions defined by the mentioned three objective functions. This algorithm requires 3 parameters including the maximum number of iterations, the number of complexes, and the number of random samples that is used to initialize each

HESSD
12, 8419–8457, 2015

complex. To ensure fair comparison, the parameters of MOSCEM-UA were set based on the number of model parameters. Therefore, the number of complexes is equal to the number of free parameters n; the number of random samples is equal to $n \cdot n \cdot 10$; and the number of iterations was set to 30 000.

3 Study site and data used

3.1 Study site

The Upper Ping River Basin (UPRB) is situated from latitude 17°14′30° to 19°47′52° N, and longitude 98°4′30° to 99°22′30° E in northern Thailand and can be separated into 14 sub-basins (Fig. 2) (Mapiam et al., 2014). It has an area of approximately 25 370 km^2 in the provinces of Chiang Mai and Lam Phun. The basin landform ranges from an undulating to a rolling terrain with steep hills of elevations of 1500 to 2000 m, and valleys of 330 to 500 m (Mapiam and Sriwongsitanon, 2009; Sriwongsitanon, 2010). The Ping River originates in Chiang Dao district, north of Chiang Mai, and flows downstream to the south to become the inflow for the Bhumiphol dam – a large dam with an active storage capacity of about 9.7 billion m^3 (Sriwongsitanon, 2010). The climate of the region is controlled by tropical monsoons. The rainy season is influenced by the southwest monsoon and brings about mild to heavy rainfall between May and October. Annual average rainfall and runoff of the UPRB are approximately 1170 and 270 mm yr^{-1}, respectively. Land cover is dominated by forest at about 86.1 % in 1988, but reduced to approximately 75.5 % in 2005, while the agricultural area increased from 9.5 % in 1988 to 18.3 % in 2005 (Sriwongsitanon and Taesombat, 2011).

HESSD
12, 8419–8457, 2015

3.2 Data collection

3.2.1 Satellite data

The satellite data used for calculating the NDII is the MODIS level 3 surface reflectance product (MOD09A1), which is at 500 m resolution in an 8 day composite of the gridded level 2 surface reflectance products. Each product pixel contains the best possible L2G observation during an 8 day period as selected on the basis of high observation coverage, low view angle, absence of clouds or cloud shadow, and aerosol loading. The MOD09 (MODIS Surface Reflectance) data product is a seven-band product, which is an estimate of the surface spectral reflectance for each band as it would have been measured at ground level as if there were no atmospheric scattering or absorption. This product has been corrected for the effects of atmospheric gases and aerosols (Vermote et al., 2011). The available MODIS data covering the UPRB from 2001 to 2013 were downloaded from http://e4ftl01.cr.usgs.gov/MOLT/MOD09A1.005/. The HDF-EOS Conversion Tool was applied to extract the desired bands (bands 2 – 841–876 nm – and 6 – 1628–1652 nm) and re-projected into Universal Transverse Mercator (Zone 47N, WGS84) from the original integerized sinusoidal (ISIN) mapping grid.

3.2.2 Rainfall data

A total of 65 non-automatic rain-gauge stations were selected from 2001 to 2013. Forty-two stations are located within the UPRB while 23 stations are situated in its surroundings. These rain-gauges are owned and operated by the Thai Meteorological Department (TMD) and the Royal Irrigation Department (RID). Quality control of the rainfall data was performed by comparing them to adjacent rainfall data. Unusual rainfall data were excluded from the analysis.

HESSD
12, 8419–8457, 2015

3.2.3 Runoff data

Daily runoff data from 1995 to 2011 at 8 stations located in the UPRB were used for FLEX^L calibration. These stations are operated by the Royal Irrigation Department (RID) in Thailand. Locations of these stations are shown in Fig. 2. Runoff data at these stations are not affected by large reservoirs and have been checked for their reliability. Catchment characteristics and data period for the selected 8 sub-basins are summarized in Table 3.

3.3 NDII drought index for the UPRB

The normalized difference infrared index (NDII) from 2001 to 2013, covering the UPRB, was computed using MODIS bands 2 and 6 reflectance data. The 8 day surface reflectance data of near infrared (band 2: wavelength between 841–876 nm) and short wave infrared (band 6: wavelength between 1628–1652 nm) are described by the Eq. (1). The 8 day NDII values were averaged over each sub-basin to allow comparison to the 8 day average S_u (root zone storage reservoir) values extracted from the FLEX^L model results at each station.

4 Results

4.1 Spatial and seasonal variation of NDII values for the UPRB and its 14 sub-basins

To demonstrate the spatial and seasonal behaviour of the NDII over the UPRB, the 8 day NDII values were aggregated to monthly values for 2001 to 2013. Figure 3 shows examples of monthly average NDII values for the UPRB in 2004, which is the year with the lowest annual average NDII value. The figure shows that NDII values are higher during the wet season (May to October) and lower during the dry season (November and April). The lower amounts of rainfall between November and April cause a continuous

HESSD
12, 8419–8457, 2015

reduction of NDII values. On the other hand, higher amounts of rainfall between May and October result in increasing NDII values. However, NDII values appear to vary little between July and October. This is likely associated with leaves being saturated with moisture during the wet period.

The average NDII values during the wet season, the dry season, and the whole year within the 13 years are presented in Table 4. The table also shows the order of the NDII values from the highest (number 1) to the lowest (number 13). It can be seen that the annual average NDII value for the whole basin is approximately 0.165, while the average values during the wet and dry season are about 0.211 and 0.118, respectively. The highest mean annual value (NDII = 0.177) occurred in 2002–2003 and the lowest (NDII = 0.149) in 2004–2005. The highest (NDII = 0.149) and lowest (NDII = 0.088) dry season values were reported in 2002–2003 and 2004–2005, respectively. On the other hand, the highest (NDII = 0.224) and lowest (NDII = 0.197) wet season values were observed in 2006–2007 and 2010–2011, respectively. It can be concluded that a dry year with relatively low moisture content and a wet year with high moisture content as specified by NDII values do not normally occur in the same year.

The 8 day NDII values were also computed for each of the 14 sub-basins within the UPRB from 2001 to 2013. Table 5 shows the monthly averaged NDII values between 2001 and 2013 and the ranking order for each of the 14 sub-basins. The results suggest that Nam Mae Taeng, Nam Mae Rim, and Upper Mae Chaem sub-basins, which have higher mean annual NDII values, have a higher moisture content than other sub-basins; while Nam Mae Haad, Nam Mae Li, and Ping River Sect. 2 are 3 sub-basins, with lower mean annual NDII values, have lower moisture content than other sub-basins. Monthly average NDII values for these 6 sub-basins are presented in Fig. 4. It can be seen that during the dry season, NDII values of the 3 sub-basins with the lowest values are a lot lower than those of the 3 sub-basins with the highest NDII values. However, NDII values for these 2 groups are not significantly different during the wet season. The figure also reveals that NDII values tend to continuously increase from relatively low values in March to higher values in June. The values slightly fluctuate during the wet

HESSD
12, 8419–8457, 2015

season before sharply falling once again when the rainy season ends, and reach their minimum values in February.

4.2 FLEX^L model results

The calibration results of FLEX^L to the sub-basins of 8 runoff stations are summarized in Table 6. The performance of the model was quite good as presented in Table 7. In Fig. 5, the duration curves of sub-basins P.20 and P.21 are presented as examples of model performance. Table 7 shows that the average Kling–Gupta efficiencies values for I_{KGE}, I_{KGL} and I_{KGF}, which indicate the performance of high flows, low flows, and flow duration curve for the 8 sub-basins. The results for the flow duration curve appear to be better than those of the high flows and especially the low flows. However, the overall results are acceptable and can be used for further analysis in this study.

4.3 Relation between NDII and root zone soil moisture storage (S_u)

The 8 day NDII values were compared to the 8 day average root zone moisture storage values of the FLEX^L model. It appeared that during moisture stress periods, the relationship could be well described by an exponential function, for each of the 8 sub-catchments. Table 8 presents the coefficients of the exponential relationships as well as the coefficients of determination (R^2) for annual, wet season, and dry season values for each sub-basin. The corresponding scatter plots are shown in Fig. 6. It can be clearly seen that the correlation is much better in the dry season than in the wet season. During the wet season, there may also be short period of moisture stress, where the exponential pattern can be recognized, but no clear relation is found when the vegetation does not experience any moisture stress.

Examples of scaled time series of NDII and root zone storage (S_u) values for the sub-catchments P.20 and P.21 are presented in Figs. 7 and 8, respectively. The scaled time series of the NDII and S_u values were calculated by dividing their value by the differences between their maximum and minimum values: $\mathrm{NDII}/(\mathrm{NDII}_{max} - -\mathrm{NDII}_{min})$ and

HESSD
12, 8419–8457, 2015

$S_u/(S_{u,\max} - S_{u,\min})$, respectively, while the maximum and the minimum are the values within the overall considered time series. Figures 7 and 8 show that the scaled NDII and S_u values are highly correlated during the dry season, but less so during the wet season. However, once the rainfall reduces significantly, even during the wet season, the NDII responds accordingly. These results confirm the potential of NDII to effectively reflect the vegetation water content, which, through the suction pressure exercised by the moisture deficit, relates to the moisture content in the root zone. During dry periods, or during dry spells in the rainy season, as soon as the leaves of the vegetation experience suction pressure, we see high values of the coefficient of determination.

If the soil moisture in the root zone is above a certain threshold value, then the leaves are not under stress. In the UPRB this situation occurs typically during the middle and late rainy season. The NDII then does not vary significantly while the root zone moisture storage may still vary, albeit above the threshold where moisture stress occurs. This causes a lower correlation between NDII and root zone storage during wet periods. However, even during the wet season dry spells can occur. We can see in Fig. 6, that during such a dry spell, the NDII and S_u again follow the exponential pattern.

5 Discussion

5.1 Is vegetation the trouble-maker or a perfect indicator for moisture storage in the root zone?

In bare soil, remote sensors can only detect soil moisture until a few centimeters below the surface (∼ 5 cm) (Entekhabi et al., 2010). Unfortunately, for hydrological modelling, the moisture state of the bare surface is of only limited interest. What is of key interest for understanding the dynamics of hydrological systems is the variability of the moisture storage in the unsaturated zone. This variability determines the rainfall–runoff behaviour, the transpiration of vegetation, and the partitioning between different hydrological fluxes. This dynamic part of the unsaturated zone is the root zone of ecosystems. However, observing the soil moisture content in the root zone is still a major challenge (Entekhabi et al., 2010).

What is normally done, is to link the moisture content of the surface layer to the total amount of moisture in the root zone. Knowing the surface soil moisture, the root zone soil moisture can be estimated by an exponential decay filter (Albergel et al., 2008; Ford et al., 2014) or by models (Reichle, 2008). However, the surface soil moisture is only weakly related with root zone soil moisture (Mahmood and Hubbard, 2007); it only works if there is connectivity between the surface and deeper layers and when a certain state of equilibrium has been reached (when the short term dynamics after a rainfall event has leveled out). It is also observed that the presence of vegetation may further deteriorate the results (Jackson and Schmugge, 1991). Avoiding the influence of surface vegetation in observing soil moisture (e.g. by SMOS or SMAP) is seen as a challenge by some in the remote sensing community (Kerr et al., 2001; Entekhabi et al., 2010). Several algorithms have been proposed to filter out the vegetation impact (Jackson and Schmugge, 1991).

In this study, we found that vegetation is not a problem, but the key to sensing the storage of moisture in the root zone. The water content in the leaves is directly connected to the suction pressure in the root zone. If the suction pressure is above a certain threshold, then this connection is direct and very sensitive. We found a highly significant correlation between NDII and S_u, particularly during periods of moisture stress. As a result, vegetation, instead of a trouble-maker in observing soil moisture, is an excellent indicator for root zone moisture storage. Observing the moisture content of vegetation provides us with directly information on the soil moisture state in the root zone. We also found that there is almost no lag time between S_u and NDII. This illustrates the fast response of vegetation to soil moisture variation, which makes the NDII a sensitive and direct indicator for root zone moisture storage.

HESSD
12, 8419–8457, 2015

5.2 Implication in hydrological modelling

An accurate simulation of root zone soil moisture is crucial in hydrological modelling (Houser et al., 1998; Western and Blöschl, 1999]. Using accurate estimates of soil moisture states would increase model performance and realism, but moreover, it would be powerful information to facilitate prediction in ungauged basins (Hrachowitz et al., 2013). However, until now, it has not been practical (e.g. Parajka et al., 2006). Assimilating soil moisture in hydrological models, either from top-soil observation by remote sensing, or from the deeper soil column by models (Reichle, 2008), is still a challenge. Several studies showed how difficult it is to assimilate soil moisture data to improve daily runoff simulation (Parajka et al., 2006). This problem is probably the result of different definitions of observed soil moisture and the soil moisture in hydrological models (Liu et al., 2012).

Soil moisture observations in the field are generally done at fixed depths within a highly heterogeneous environment, while vegetation does not root at fixed depths. Vegetation extends its roots in the 3-dimensional environment in such a way as to guarantee sufficient storage to overcome critical periods of droughts (Gao et al., 2014b). This root zone storage is precisely the dynamic part of the unsaturated zone, represented by the unsaturated reservoir in conceptual hydrological models such as presented in Fig. 1. This is probably why such a good correlation is found between the NDII and S_u, while this may be less so with observations at fixed depths.

By observing the moisture content of the leaves, the NDII represents the soil moisture storage condition of the entire root zone, which is precisely the information that hydrological models require. This study clearly shows the strong temporal correlation between S_u and NDII. From the relationship between NDII and S_u, we can directly derive a proxy for the soil moisture state, which can potentially be assimilated in hydrological models. This method would be extremely useful for prediction of discharge in ungauged basins.

HESSD
12, 8419–8457, 2015

We should, of course, be aware of regional limitations. This study considered a tropical seasonal ecosystem, where periods of moisture stress regularly occur. We need further investigations into the usefulness of this approach in catchments with different climates.

6 Conclusions

The Normalized Difference Infrared Index (NDII) was used to investigate drought for the Upper Ping River Basins (UPRB) from 2001 to 2013. Monthly average NDII values appear to be spatially distributed over the UPRB, in agreement with seasonal variability and landscape characteristics. NDII values appear to be lower during the dry season and higher during the wet season as a result of increasing basin moisture content influenced by the high amount of rainfall in the wet season. The NDII appears to correlate very well with the moisture storage in the root zone, offering an interesting proxy variable for calibration of hydrological models in ungauged basins.

To illustrate the importance of NDII as a proxy for soil moisture storage in hydrological models, we applied FLEX^L model to assess the root zone soil moisture content (S_u) at 8 runoff stations in the UPRB. The results show that the 8 day average NDII values over the study sub-basin correlate very well with the 8 day average S_u for all sub-catchments during the dry season (average R^2 equals 0.87), and less so during the wet season (average R^2 equals 0.61). However, the correlations during the wet season is still significant meaning that NDII can still be used to reflect the root zone moisture content during dry spells when leaves are under moisture stress. Hence, the natural interaction between rainfall, soil moisture, and leave water content can be visualised by the NDII, making it an important indicator both for hydrological modelling and drought assessment.

Acknowledgements. We gratefully acknowledge Kasetsart University Research and Development Institute for financially supporting this research. We also appreciate RID and TMD for providing the rainfall data. Finally, we sincerely thank the MODIS Land Discipline Group for creating and sharing the MODIS LAND data used in this study.

References

Albergel, C., Rüdiger, C., Pellarin, T., Calvet, J.-C., Fritz, N., Froissard, F., Suquia, D., Petitpa, A., Piguet, B., and Martin, E.: From near-surface to root-zone soil moisture using an exponential filter: an assessment of the method based on in-situ observations and model simulations, Hydrol. Earth Syst. Sci., 12, 1323–1337, doi:10.5194/hess-12-1323-2008, 2008.

Ceccato, P., Flasse, S., Tarantola, S., Jacquemoud, S., and Grégoire, J. M.: Detecting vegetation leaf water content using reflectance in the optical domain, Remote Sens. Environ., 77, 22–33, doi:10.1016/S0034-4257(01)00191-2, 2001.

Ceccato, P., Flasse, S., and Grégoire, J. M.: Designing a spectral index to estimate vegetation water content from remote sensing data: Part 2, Validations and applications, Remote Sens. Environ., 82, 198–207, doi:10.1016/S0034-4257(02)00036-6, 2002.

Cheng, Y. B., Zarco-Tejada, P. J., Riaño, D., Rueda, C. A., and Ustin, S. L.: Estimating vegetation water content with hyperspectral data for different canopy scenarios: relationships between AVIRIS and MODIS indexes, Remote Sens. Environ., 105, 354–366, doi:10.1016/j.rse.2006.07.005, 2006.

de Groen, M. M. and Savenije, H. H. G.: A monthly interception equation based on the statistical characteristics of daily rainfall, Water Resour. Res., 42, W12417, doi:10.1029/2006WR005013, 2006.

De Jeu, R. A. M., Wagner, W., Holmes, T. R. H., Dolman, A. J., van de Giesen, N. C., and Friesen, J.: Global soil moisture patterns observed by space borne microwave radiometers and scatterometers, Surv. Geophys., 28, 399–420, doi:10.1007/s10712-008-9044-0, 2008.

Entekhabi, D., Nioku, E. G., O'Neill, P. E., Kellogg, K. H., Crow, W. T., Edelstein, W. N., Entin, J. K., Goodman, S. D., Jackson, T. J., Johnson, J., Kimball, J., Piepmeier, J. R., Koster, R. D., Martin, N., McDonald, K. C., Moghaddam, M., Moran, S., Reichle, R., Shi, J.-C., Spencer, M. W., Thurman, S. W., Leung, T., and Van Zyl, J.: The Soil Moisture Active Passive (SMAP) Mission, Proc. IEEE, 98, 704–716, 2010.

HESSD
12, 8419–8457, 2015

Fenicia, F., Kavetski, D., and Savenije, H. H. G.: Elements of a flexible approach for conceptual hydrological modeling: 1. Motivation and theoretical development, Water Resour. Res., 47, W11510, doi:10.1029/2010WR010174, 2011.
Fensholt, R. and Sandholt, I.: Derivation of a shortwave infrared stress index from MODIS near- and shortwave infrared data in a semiarid environment, Remote Sens. Environ., 87, 111–121, doi:10.1016/j.rse.2003.07.002, 2003.
Ford, T. W., Harris, E., and Quiring, S. M.: Estimating root zone soil moisture using near-surface observations from SMOS, Hydrol. Earth Syst. Sci., 18, 139–154, doi:10.5194/hess-18-139-2014, 2014.
Friesen, J., Steele-Dunne, S. C., and van de Giesen, N.: Diurnal differences in global ERS scatterometer backscatter observations of the land surface, IEEE T. Geosci. Remote, 50, 2595–2602, 2012.
Gao, B. C.: NDWI – a normalized difference water index for remote sensing of vegetation liquid water from space, Remote Sens. Environ., 58, 257–266, doi:10.1016/S0034-4257(96)00067-3, 1996.
Gao, B. C. and Goetz, A. F. H.: Retrieval of equivalent water thickness and information related to biochemical components of vegetation canopies from AVIRIS data, Remote Sens. Environ., 52, 155–162, doi:10.1016/0034-4257(95)00039-4, 1995.
Gao, H., Hrachowitz, M., Fenicia, F., Gharari, S., and Savenije, H. H. G.: Testing the realism of a topography-driven model (FLEX-Topo) in the nested catchments of the Upper Heihe, China, Hydrol. Earth Syst. Sci., 18, 1895–1915, doi:10.5194/hess-18-1895-2014, 2014a.
Gao, H., Hrachowitz, M., Schymanski, S. J., Fenicia, F., Sriwongsitanon, N., and Savenije, H. H. G.: Climate controls how ecosystems size the root zone storage capacity at catchment scale, Geophys. Res. Lett., 41, 7916–7923, doi:10.1002/2014GL061668, 2014b.
Gao, H., Hrachowitz, M., Sriwongsitanon, N., Fenicia, F., Gharari, S., and Savenije, H. H. G.: Accounting for the influence of vegetation and topography improves model transferability, Water Resour. Res., in review, 2015.
Gupta, H. V., Kling, H., Yilmaz, K. K., and Martinez, G. F.: Decomposition of the mean squared error and NSE performance criteria: implications for improving hydrological modeling, J. Hydrol., 377, 80–91, doi:10.1016/j.jhydrol.2009.08.003, 2009.
Houser, P. R., Shuttleworth, W. J., Famiglietti, J. S., Gupta, H. V., Syed, K. H., and Goodrich, D. C.: Integration of soil moisture remote sensing and hydrologic modeling using data assimilation, Water Resour. Res., 34, 3405–3420, doi:10.1029/1998WR900001, 1998.

Hunt Jr., E. R. and Rock, B. N.: Detection of changes in leaf water content using near- and middle-infrared reflectances, Remote Sens. Environ., 30, 43–54, doi:10.1016/0034-4257(89)90046-1, 1989.
Hrachowitz, M., Savenije, H. H. G., Blöschl, G., McDonnell, J. J., Sivapalan, M., Pomeroy, J. W., Arheimer, B., Blume, T., Clark, M. P., Ehret, U., Fenicia, F., Freer, J. E., Gelfan, A., Gupta, H. V., Hughes, D. A., Hut, R. W., Montanari, A., Pande, S., Tetzlaff, D., Troch, P. A., Uhlenbrook, S., Wagener, T., Winsemius, H. C., Woods, R. A., Zehe, E., and Cudennec, C.: A decade of predictions in ungauged basins (PUB); a review, Hydrolog. Sci. J., 58, 1–58, doi:10.1080/02626667.2013.803183, 2013.
Jackson, T. J. and Schmugge, T. J.: Vegetation effects on the microwave emission of soils, Remote Sens. Environ., 36, 203–212, 1991.
Kerr, Y. H., Waldteufel, P., Wigneron, J.-P., Martinuzzi, J.-M., Font, J., and Berger, M.: Soil moisture retrieval from space: the Soil Moisture and Ocean Salinity (SMOS) mission, IEEE T. Geosci. Remote, 39, 1729–1735, 2001.
Korres, W., Reichenau, T. G., Fiener, P., Koyama, C. N., Bogena, H. R., Cornelissen, T., Baatz, R., Herbst, M., Diekkrüger, B., Vereecken, H., and Schneider, K.: Spatio-temporal soil moisture patterns – a meta-analysis using plot to catchment scale data, J. Hydrol., 520, 326–341, doi:10.1016/j.jhydrol.2014.11.042, 2015.
Legates, D. R., Mahmood, R., Levia, D. F., DeLiberty, T. L., Quiring, S. M., Houser, C., and Nelson, F. E.: Soil moisture: a central and unifying theme in physical geography, Prog. Phys. Geogr., 35, 65–86, 2011.
Liang, X., Lettenmaier, D. P., Wood, E. F., and Burges, S. J.: A simple hydrologically based model of land surface water and energy fluxes for general circulation models, J. Geophys. Res., 99, 14415–14428, 1994.
Liu, Y., Weerts, A. H., Clark, M., Hendricks Franssen, H.-J., Kumar, S., Moradkhani, H., Seo, D.-J., Schwanenberg, D., Smith, P., van Dijk, A. I. J. M., van Velzen, N., He, M., Lee, H., Noh, S. J., Rakovec, O., and Restrepo, P.: Advancing data assimilation in operational hydrologic forecasting: progresses, challenges, and emerging opportunities, Hydrol. Earth Syst. Sci., 16, 3863–3887, doi:10.5194/hess-16-3863-2012, 2012.
Mahmood, R. and Hubbard, K. G.: Relationship between soil moisture of near surface and multiple depths of the root zone under heterogeneous land uses and varying hydroclimatic conditions, Hydrol. Process., 25, 3449–3462, doi:10.1002/hyp.6578, 2007.

Mapiam, P. P. and Sriwongsitanon, N.: Estimation of the URBS model parameters for flood estimation of ungauged catchments in the upper Ping river basin, Thailand, Science Asia, 35, 49–56, 2009.
Mapiam, P. P., Sharma, A., and Sriwongsitanon, N.: Defining the $Z \sim R$ relationship using gauge rainfall with coarse temporal resolution: implications for flood forecast, J. Hydrol. Eng., 19, 04014004, doi:10.1061/(ASCE)HE.1943-5584.0000616, 2014.
Maselli, F.: Monitoring forest conditions in a protected Mediterranean coastal area by the analysis of multiyear NDVI data, Remote Sens. Environ., 89, 423–433, doi:10.1016/j.rse.2003.10.020, 2004.
Parajka, J., Naeimi, V., Blöschl, G., Wagner, W., Merz, R., and Scipal, K.: Assimilating scatterometer soil moisture data into conceptual hydrologic models at the regional scale, Hydrol. Earth Syst. Sci., 10, 353–368, doi:10.5194/hess-10-353-2006, 2006.
Peñuelas, J., Filella, I., Biel, C., Serrano, L., and Savé, R.: The reflectance at the 950–970 nm region as an indicator of plant water status, Int. J. Remote Sens., 14, 1887–1905, doi:10.1080/01431169308954010, 1993.
Porporato, A., Daly, E., and Rodriguez-Iturbe, I.: Soil water balance and ecosystem response to climate change, Am. Nat., 164, 625–623, 2004.
Reichle, R. H.: Data assimilation methods in the Earth sciences, Adv. Water Resour., 31, 1411–1418, 2008.
Rhee, J., Im, J., and Carbone, G. J.: Monitoring agricultural drought for arid and humid regions using multi-sensor remote sensing data, J. Hydrol., 114, 2875–2887, doi:10.1016/j.rse.2010.07.005, 2010.
Rouse, J. W., Hass, R. H., Schell, J. A., and Deering, D. W.: Monitoring vegetation systems in the Great Plains with ERTS, NASA SP-351, Proceedings of the 3rd Earth Resources Technology Satellite-1 symposium, Greenbelt, MD, 309–317, 1974.
Shi, J., Wang, J., Hsu, A. Y., O'Neill, P. E., and Engman, E. T.: Estimation of bare surface soil moisture and surface roughness parameter using L-band SAR image data, IEEE T. Geosci. Remote, 35, 1254–1266, 1997.
Sriwongsitanon, N.: Flood forecasting system development for the Upper Ping River Basin, Nat. Sci., 44, 717–731, 2010.
Sriwongsitanon, N. and Taesombat, W.: Effects of land cover on runoff coefficient, J. Hydrol., 410, 226–238, doi:10.1016/j.jhydrol.2011.09.021, 2011.

Steele-Dunne, S. C., Friesen, J., and van de Giesen, N.: Using Diurnal Variation in Backscatter to Detect Vegetation Water Stress, IEEE T. Geosci. Remote, 50, 2618–2629, 2012.
Tucker, C. J.: Remote sensing of leaf water content in the near infrared, Remote Sens. Environ., 10, 23–32, doi:10.1016/0034-4257(80)90096-6, 1980.
Ustin, S. L., Roberts, D. A., Gamon, J. A., Asner, G. P., and Green, R. O.: Using imaging spectroscopy to study ecosystem processes and properties, BioScience, 54, 523–534, doi:10.1641/0006-3568(2004)054[0523:UISTSE]2.0.CO;2, 2004.
Van Emmerik, T., Steele-Dunne, S. C., Judge, J., and van de Giesen, N. C.: Impact of diurnal variation in vegetation water content on radar backscatter from maize during water stress, IEEE T. Geosci. Remote, 53, 3855–3869, doi:10.1109/TGRS.2014.2386142, 2015.
Vermote, E. F., Kotchenova, S. Y., and Ray, J. P.: MODIS Surface Reflectance User's Guide, available at: http://modis-sr.ltdri.org (last access: August 2015), 2011.
Vrugt, J. A., Gupta, H. V., Bastidas, L. A., Bouten, W., and Sorooshian, S.: Effective and efficient algorithm for multiobjective optimization of hydrologic models, Water Resour. Res., 39, 1214, doi:10.1029/2002WR001746, 2003.
Wang, K., Wang, P., Li, Z., Cribb, M., and Sparrow, M.: A simple method to estimate actual evapotranspiration from a combination of net radiation, vegetation index, and temperature, J. Geophys. Res., 112, D15107, doi:10.1029/2006JD008351, 2007.
Western, A. W. and Blöschl, G.: On the spatial scaling of soil moisture, J. Hydrol., 217, 203–224, 1999.
Yilmaz, M. T., Hunt Jr., E. R., and Jackson, T. J.: Remote sensing of vegetation water content from equivalent water thickness using satellite imagery, Remote Sens. Environ., 112, 2514–2522, doi:10.1016/j.rse.2007.11.014, 2008.
Zhao, R. J.: The Xinanjiang model applied in China, J. Hydrol., 135, 371–381, doi:10.1016/0022-1694(92)90096-E, 1992.

Table 1. Water balance and constitutive equations used in $FLEX^L$.

Reservoirs	Water balance equations	Equation	Constitutive equations	Equation
Interception	$\frac{dS_i}{dt} = P - E_i - P_e$	(2)	$E_i = \begin{cases} E_0; & S_i > 0 \\ 0; & S_i = 0 \end{cases}$	(3)
			$P_e = \begin{cases} 0; & S_i < S_{i,\max} \\ P; & S_i = S_{i,\max} \end{cases}$	(4)
Unsaturated reservoir	$\frac{dS_u}{dt} = P_e - R - E_t$	(5)	$\frac{R}{P_e} = 1 - \left(1 - \frac{S_u}{(1+\beta)S_{u,\max}}\right)^{\beta}$	(6)
			$E_t = (E_0 - E_i)\cdot\min\left(1, \frac{S_u}{C_e S_{u,\max}(1+\beta)}\right)$	(7)
Splitter and Lag function			$R_f = R \cdot D$	(8)
			$R_s = R \cdot (1 - D)$	(9)
			$R_{fl}(t) = \sum_{i=1}^{T_{lag}} c(i) \cdot R_f(t - i + 1)$	(10)
			$c(i) = i / \sum_{u=1}^{T_{lag}} u$	(11)
Fast reservoir	$\frac{dS_f}{dt} = R_{fl} - Q_{ff} - Q_f$	(12)	$Q_{ff} = \max(0, S_f - S_{f,\max})/K_{ff}$	(13)
			$Q_f = S_f / K_f$	(14)
Slow reservoir	$\frac{dS_s}{dt} = R_s - Q_s$	(15)	$Q_s = S_s / K_s$	(16)

HESSD
12, 8419–8457, 2015

Table 2. Parameter range of the FLEX^L model.

Parameter	Range	Parameters	Range
$S_{i,\,max}$ (mm)	(0.1, 6)	K_{ff} (d)	(1, 9)
$S_{u,\,max}$ (mm)	(10, 1000)	T_{lagF} (d)	(0, 5)
β (–)	(0, 2)	T_{lagS} (d)	(0, 5)
C_e (–)	(0.1, 0.9)	K_f (d)	(1, 40)
D (–)	(0, 1)	K_s (d)	(10, 500)
$S_{f,\,max}$ (mm)	(10, 200)		

After Gao et al. (2015).

HESSD
12, 8419–8457, 2015

Table 3. Catchment characteristics and data period for selected 8 sub-basins in the UPRB.

Sub-basin	Mae Taeng at Ban Mae Taeng (P.4A)	Nam Mae Chaem at Kaeng Ob Luang (P.14)	Ping River at Chiang Dao (P.20)	Nam Mae Rim at Ban Rim Tai (P.21)	Nam Mae Klang at Pracha Uthit Bridge (P.24A)	Nam Mae Khan at Ban Klang (P.71)	Nam Mae Li at Ban Mae E Hai (P.76)	Nam Mae Tha at Ban Sop Mae Sapuad (P.77)
Area (km^2)	1902	3853	1355	515	460	1771	1541	547
Altitude range (m)	1020	991	790	731	888	828	618	641
Average channel slope (%)	0.78	0.81	0.80	0.72	0.98	0.69	0.41	0.63
Average forest and agricultural areas (%)	81.9, 16.5	91.8, 7.4	80.9, 12.8	86.1, 11.6	79.7, 14.2	86.1, 10.1	69.7, 20.1	80.4, 12.7
Average rainfall depth (wet season/dry season) (mm)	953 (88 %) 130 (12 %)	883 (92 %) 75 (8 %)	1076 (88 %) 150 (12 %)	1019 (90 %) 115 (10 %)	860 (88 %) 121 (12 %)	1090 (89 %) 132 (11 %)	1092 (91 %) 106 (9 %)	757 (88 %) 88 (10 %)
Number of years data is coincident with NDII	11	7	12	11	12	9	12	12
Data period	1995–2011	1995–2007	1995–2012	1995–2011	1995–2012	1996–2009	1996–2012	1996–2012

HESSD
12, 8419–8457, 2015

Table 4. Average NDII values during the wet season, the dry season, and the whole year from 2001 to 2013, and their order of moisture content (range from 1 to 13. Less value indicates less NDII) for the entire Upper Ping River Basin.

Year	Wet season (May–Oct)	Dry season (Nov–Apr)	Annual
2001–2002	0.223 (2)	0.119 (7)	0.171 (4)
2002–2003	0.205 (9)	0.149 (1)	0.177 (1)
2003–2004	0.218 (5)	0.091 (12)	0.155 (12)
2004–2005	0.210 (8)	0.088 (13)	0.149 (13)
2005–2006	0.200 (11)	0.128 (3)	0.164 (7)
2006–2007	0.224 (1)	0.111 (10)	0.168 (5)
2007–2008	0.222 (3)	0.130 (2)	0.176 (2)
2008–2009	0.221 (4)	0.123 (5)	0.172 (3)
2009–2010	0.213 (7)	0.101 (11)	0.157 (11)
2010–2011	0.197 (13)	0.128 (4)	0.163 (8)
2011–2012	0.216 (6)	0.116 (9)	0.166 (6)
2012–2013	0.201 (10)	0.118 (8)	0.159 (10)
2013–2014	0.199 (12)	0.123 (6)	0.161 (9)
Average	0.211	0.118	0.165
Maximum	0.224	0.149	0.177
Minimum	0.197	0.088	0.149

HESSD
12, 8419–8457, 2015

Table 5. Monthly average NDII values between 2001 and 2013 and the order of basin moisture content for each of 14 sub-basins within the UPRB.

Sub-basin	Jan	Feb	Mar	Apr	May	Jun	Jul	Aug	Sep	Oct	Nov	Dec	Average
Ping River Sect. 1	0.14(7.5)	0.06(7.4)	0.02(8.8)	0.07(8.9)	0.17(8.4)	0.21(6.2)	0.22(4.5)	0.22(6.1)	0.24(7.5)	0.23(8.3)	0.22(7.8)	0.18(7.2)	0.16(8)
Nam Mae Ngad	0.17(5.2)	0.11(5.9)	0.07(6.2)	0.10(6.3)	0.18(6.9)	0.21(7.1)	0.21(7.5)	0.22(8.0)	0.23(9.2)	0.23(7.9)	0.23(6.4)	0.20(5.7)	0.18(6)
Nam Mae Taeng	0.21(1.3)	0.16(1.0)	0.13(1.2)	0.14(2.1)	0.19(3.9)	0.21(6.1)	0.22(6.0)	0.23(4.5)	0.25(3.1)	0.25(2.6)	0.26(1.2)	0.24(1.7)	0.21(1)
Ping River Sect. 2	0.07(11.5)	0.02(9.8)	0.01(9.2)	0.04(11.6)	0.13(13.1)	0.18(13.0)	0.18(13.5)	0.19(13.3)	0.21(13.6)	0.21(12.7)	0.17(13.4)	0.12(13.5)	0.13(12)
Nam Mae Rim	0.17(5.3)	0.13(4.3)	0.10(3.9)	0.13(3.3)	0.20(2.6)	0.22(3.7)	0.22(4.0)	0.24(2.5)	0.26(1.3)	0.26(1.2)	0.24(3.7)	0.20(5.6)	0.20(2)
Nam Mae Kuang	0.09(9.4)	0.03(9.5)	0.02(9.3)	0.05(10.1)	0.15(10.0)	0.20(8.1)	0.21(8.1)	0.22(8.2)	0.24(7.0)	0.23(7.5)	0.20(10.4)	0.14(10.7)	0.15(9)
Nam Mae Ngan	0.18(4.0)	0.13(4.4)	0.10(4.9)	0.13(4.1)	0.19(3.9)	0.21(5.3)	0.22(5.5)	0.23(5.2)	0.25(3.9)	0.24(4.5)	0.24(4.5)	0.22(4.0)	0.19(5)
Nam Mae Li	0.05(12.5)	−0.04(12.5)	−0.04(12.7)	0.02(12.1)	0.14(11.9)	0.19(11.8)	0.20(9.7)	0.23(8.3)	0.23(9.9)	0.21(13.0)	0.18(13.2)	0.13(12.5)	0.12(13)
Nam Mae Klang	0.19(3.3)	0.13(3.5)	0.12(2.8)	0.14(2.3)	0.20(2.9)	0.22(4.8)	0.22(7.2)	0.23(7.6)	0.23(8.6)	0.24(7.2)	0.24(4.5)	0.22(3.3)	0.20(4)
Ping River Sect. 3	0.06(11.7)	−0.03(12.5)	−0.04(12.3)	0.03(11.2)	0.15(9.3)	0.21(7.2)	0.21(8.7)	0.21(9.9)	0.22(11.4)	0.21(11.9)	0.19(11.2)	0.15(10.3)	0.13(11)
Upper Nam Mae Chaem	0.20(1.9)	0.15(2.0)	0.12(2.3)	0.13(4.2)	0.18(6.7)	0.20(9.5)	0.21(9.2)	0.21(9.1)	0.24(6.2)	0.25(3.9)	0.26(2.1)	0.24(1.6)	0.20(3)
Lower Nam Mae Chaem	0.09(9.8)	0.006(10.7)	−0.007(10.8)	0.05(10.2)	0.15(10.2)	0.20(10.2)	0.20(9.9)	0.21(8.9)	0.23(9.5)	0.23(8.3)	0.21(8.9)	0.16(9.2)	0.14(10)
Nam Mae Haad	0.03(14.0)	−0.07(14.0)	−0.06(13.8)	0.003(12.9)	0.15(10.0)	0.21(5.8)	0.22(6.4)	0.23(6.2)	0.24(5.2)	0.22(9.7)	0.19(11.2)	0.12(12.4)	0.12(14)
Nam Mae Tuen	0.13(7.6)	0.05(7.7)	0.05(7.0)	0.10(5.9)	0.19(5.2)	0.21(6.2)	0.22(4.9)	0.222(7.2)	0.23(8.7)	0.24(6.2)	0.23(6.5)	0.20(6.5)	0.17(7)
Average	0.13	0.06	0.04	0.08	0.17	0.20	0.21	0.22	0.24	0.23	0.22	0.18	0.16
Maximum	0.21	0.16	0.13	0.14	0.20	0.22	0.22	0.24	0.26	0.26	0.26	0.24	0.21
Minimum	0.03	−0.07	−0.06	0.003	0.13	0.18	0.18	0.19	0.21	0.21	0.17	0.12	0.12

HESSD
12, 8419–8457, 2015
NDII as a proxy for soil moisture storage in hydrological modelling
N. Sriwongsitanon et al.

Table 6. $FLEX^L$ parameters calibrated at 8 runoff stations located in the UPRB.

Runoff station	$S_{i,\,max}$ (mm)	$S_{u,\,max}$ (mm)	Ce (–)	Beta (–)	D (–)	K_f (days)	K_s (days)	T_{lagF} (days)	T_{lagS} (days)	$S_{f,\,max}$ (mm)	K_{ff} (days)
P.4A	2.0	463	0.30	0.66	0.77	2.9	42	1.1	49	93	9.1
P.14	2.3	269	0.55	1.16	0.65	4.0	63	1.5	39	155	7.6
P.21	2.3	388	0.31	0.90	0.64	2.1	66	2.4	48	33	2.5
P.20	2.0	324	0.47	0.50	0.79	7.7	103	1.0	25	69	1.7
P.24A	3.2	209	0.77	1.53	0.89	3.2	267	1.5	44	24	4.2
P.76	2.3	486	0.62	0.32	0.89	2.4	191	2.7	3	130	7.4
P.77	4.5	344	0.48	0.27	0.75	1.5	65	1.2	30	164	5.6
P.71	4.3	532	0.34	0.46	0.90	3.5	80	1.8	15	179	6.5

Discussion Paper | Discussion Paper | Discussion Paper | Discussion Paper

HESSD

12, 8419–8457, 2015

NDII as a proxy for soil moisture storage in hydrological modelling

N. Sriwongsitanon et al.

Table 7. FLEX^L model performance at 8 runoff stations.

Station	Data period	I_{KGE}	I_{KGL}	I_{KGF}
P.4A	1995–2009	0.822	0.667	0.963
P.14	1995–2007	0.796	0.442	0.966
P.21	1995–2009	0.814	0.718	0.985
P.20	1995–2011	0.792	0.685	0.964
P.24A	1995–2011	0.623	0.598	0.945
P76	2000–2011	0.539	0.665	0.916
P.77	1999–2011	0.775	0.612	0.970
P.71	1996–2009	0.823	0.714	0.975
Average		0.748	0.638	0.961

HESSD
12, 8419–8457, 2015

Table 8. Exponential relationships between the average NDII values and simulated root zone moisture storage (S_u) in the 8 sub-basins controlled by the 8 runoff stations.

Runoff station	Annual relationship			Wet season relationship			Dry season relationship		
	a	b	R^2	a	b	R^2	a	b	R^2
P.4A	11.2	12.4	0.66	11.1	12.9	0.53	12.6	11.2	0.90
P.14	21.9	9.8	0.81	19.2	10.8	0.71	24.6	8.5	0.92
P.20	52.3	7.4	0.79	36.2	9.1	0.72	59.7	6.7	0.91
P.21	30.8	9.0	0.68	27.8	9.3	0.53	30.6	9.22	0.86
P.24A	22.1	8.5	0.60	24.2	8.3	0.41	22.4	8.1	0.81
P.71	2.1	19.9	0.77	1.9	20.5	0.65	2.3	19.0	0.87
P.76	10.1	13.6	0.85	8.1	14.4	0.74	10.8	14.6	0.87
P.77	35.4	8.0	0.70	20.7	10.2	0.61	40.6	7.7	0.83
Average	–	–	0.73	–	–	0.61	–	–	0.87

Note: $S_u = ae^{bNDII}$.

HESSD
12, 8419–8457, 2015

NDII as a proxy for soil moisture storage in hydrological modelling

N. Sriwongsitanon et al.

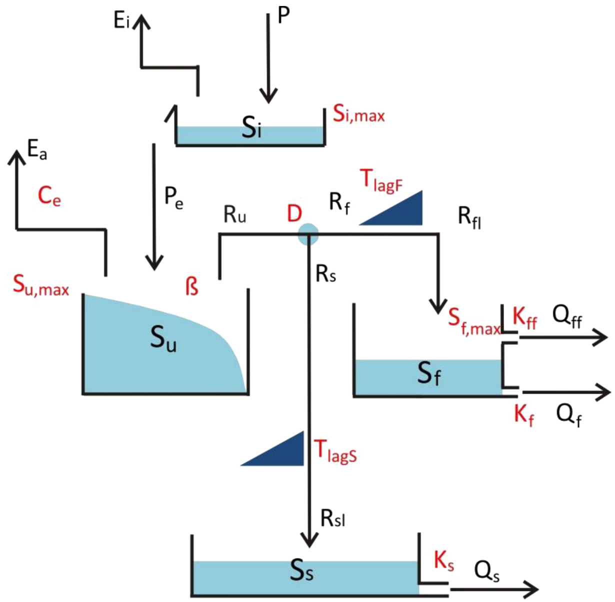

Figure 1. Model structure of the FLEX^{L}.

HESSD
12, 8419–8457, 2015

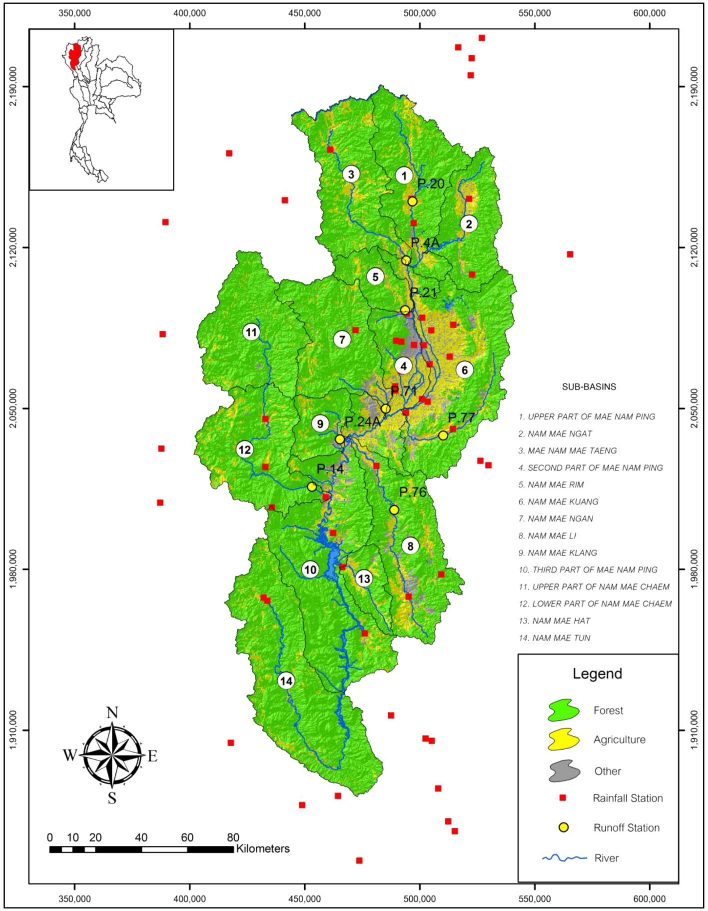

Figure 2. The Upper Ping River Basin (UPRB) and the locations of the rain-gauge and runoff stations. The numbers indicate the 14 sub-basins of the UPRB.

HESSD
12, 8419–8457, 2015

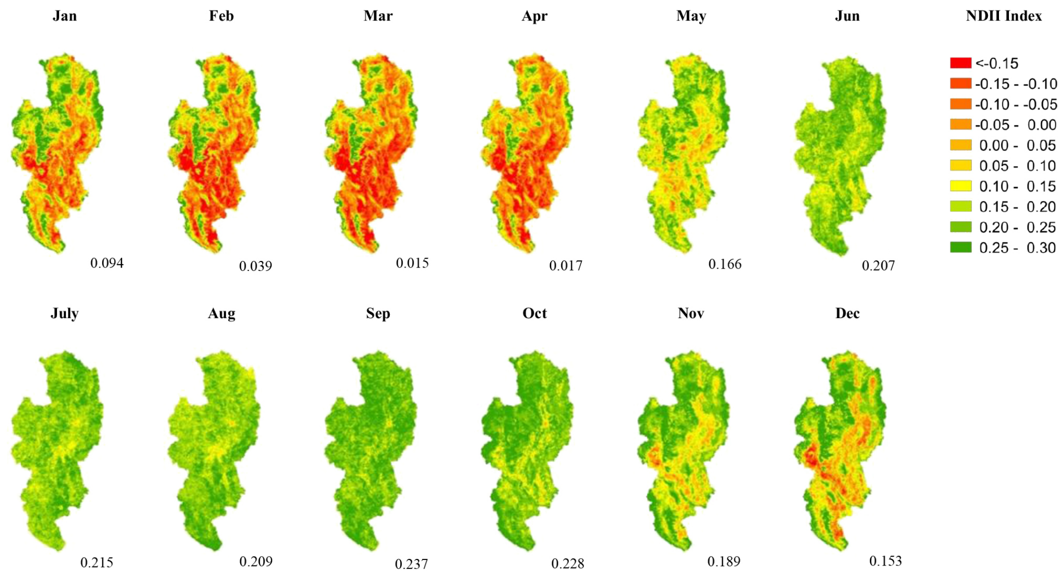

Figure 3. Monthly average NDII values for the UPRB in 2004. The green color indicates an NDII between 0.15 and 0.30, yellow between 0 and 0.15, orange between −0.15 and 0 and red an NDII < −0.15) representing relatively high-, medium-, low-, and very low- root zone moisture content.

HESSD
12, 8419–8457, 2015

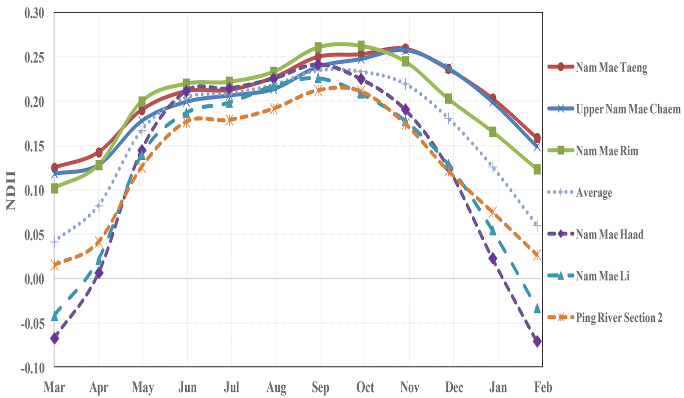

Figure 4. Monthly average NDII values for 6 sub-basins compared to the basin average in the UPRB.

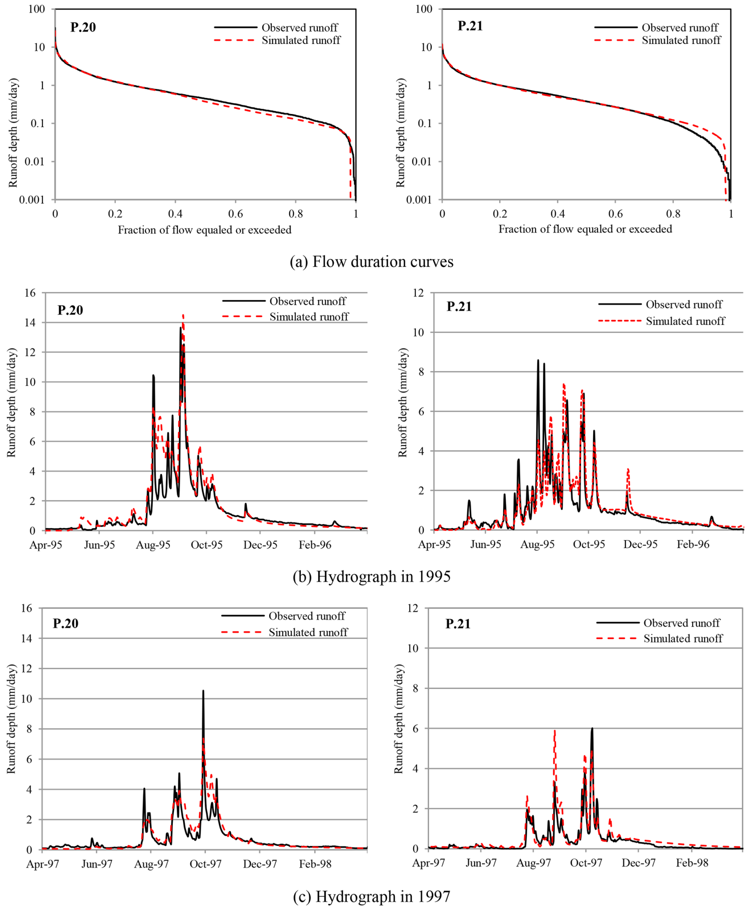

Figure 5. Examples of flow duration curves and simulated hydrographs using FLEX^L at runoff stations P.20 and P.21.

HESSD
12, 8419–8457, 2015

HESSD
12, 8419–8457, 2015

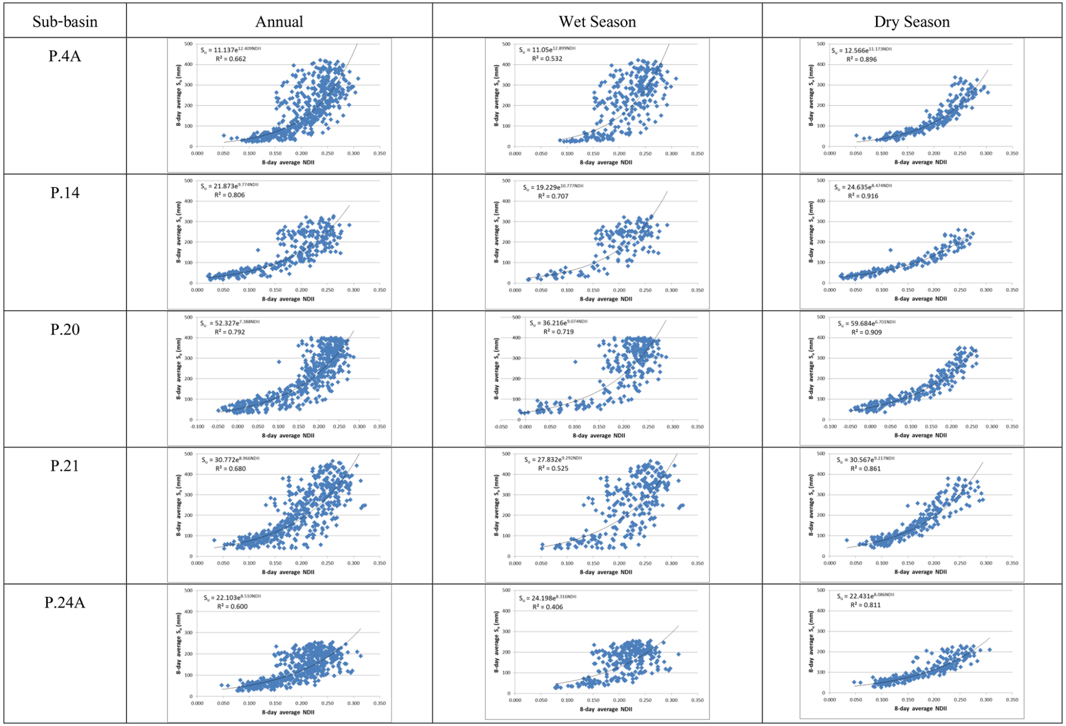

Figure 6.

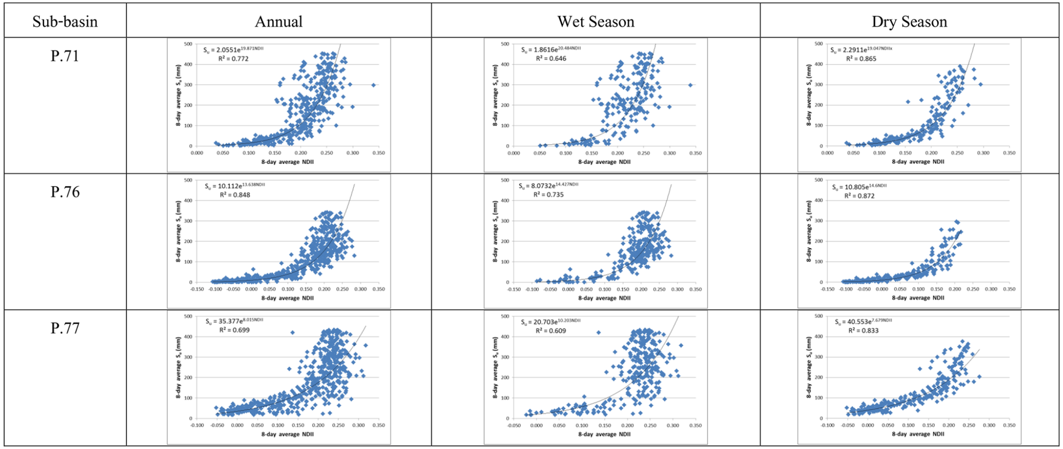

Figure 6. Scatter plots between the average NDII and the average soil moisture storage in the root zone reservoir (S_u) for 8 sub-basins controlled by runoff stations.

HESSD
12, 8419–8457, 2015

NDII as a proxy for soil moisture storage in hydrological modelling

N. Sriwongsitanon et al.

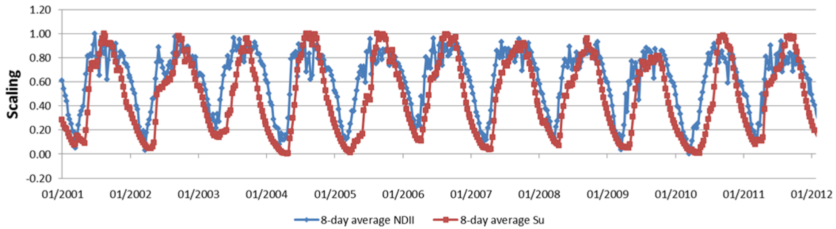

(a) Annual scaled time series

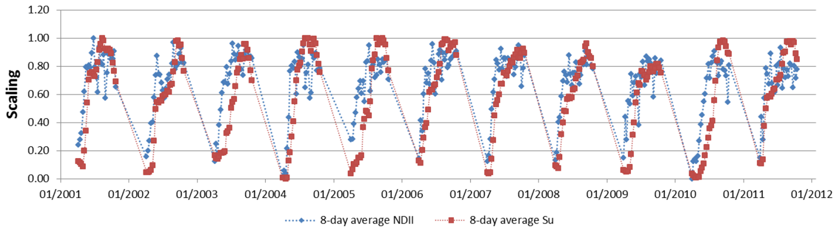

(b) Scaled time series in wet seasons

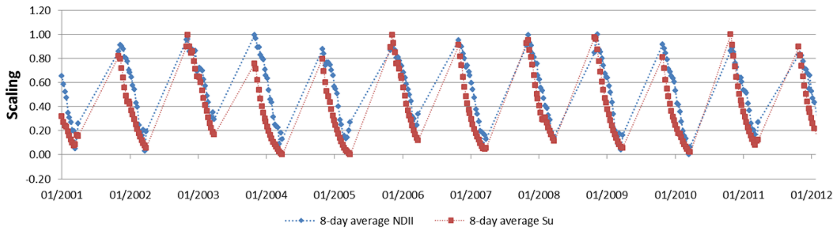

(c) Scaled time series in dry seasons

Figure 7. Scaled time series of the average NDII values compared to the average root zone moisture storage (S_u) in the sub-basin of the Ping River controlled by Chiang Dao (P.20) runoff station.

HESSD
12, 8419–8457, 2015

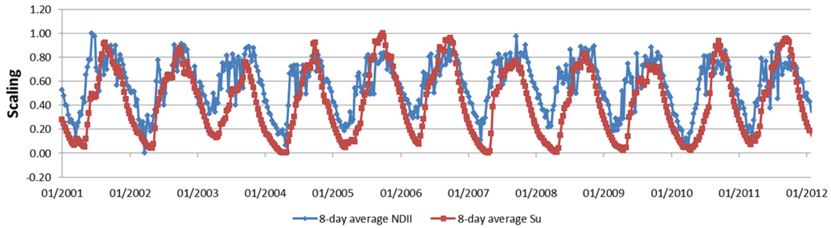

(a) Annual scaled time series

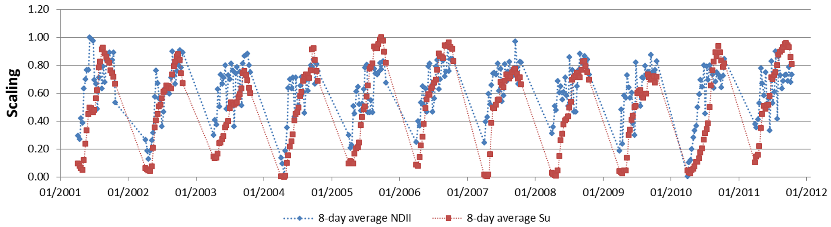

(b) Scaled time series in wet seasons

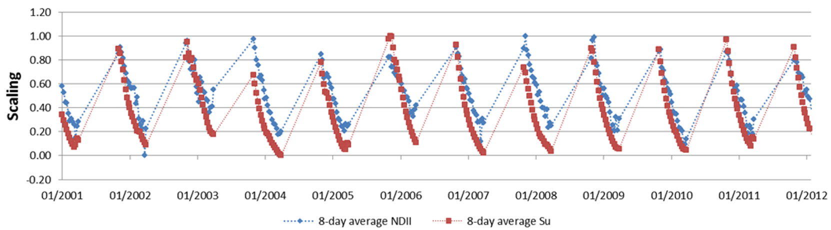

(c) Scaled time series in dry seasons

Figure 8. Scaled time series of the average NDII values compared to the average root zone moisture storage (S_u) in Nam Mae Rim sub-basin at Ban Rim Tai (P.21) runoff station.

HESSD
12, 8419–8457, 2015